PRIMARY RESEARCH ARTICLE

WILEY Global Change Biology

Tundra landscape heterogeneity, not interannual variability, controls the decadal regional carbon balance in the Western Russian Arctic

Claire C. Treat[1] | Maija E. Marushchak[1] | Carolina Voigt[1] | Yu Zhang[2] |

Zeli Tan[3,4] | Qianlai Zhuang[4] | Tarmo A. Virtanen[5] | Aleksi Räsänen[5,6] |

Christina Biasi[1] | Gustaf Hugelius[7] | Dmitry Kaverin[8] | Paul A. Miller[9] |

Martin Stendel[10] | Vladimir Romanovsky[11,12] | Felix Rivkin[13] | Pertti J. Martikainen[1] |

Narasinha J. Shurpali[1]

[1]Biogeochemistry Research Group, Department of Biological and Environmental Sciences, University of Eastern Finland, Kuopio, Finland

[2]Canada Centre for Mapping and Earth Observation, Natural Resources Canada, Ottawa, Ontario

[3]Pacific Northwest National Laboratory, Richland, Washington

[4]Department of Earth, Atmospheric, and Planetary Sciences, Purdue University, West Lafayette, Indiana

[5]Ecosystems and Environment Research Programme, Faculty of Biological and Environmental Sciences, University of Helsinki, Helsinki, Finland

[6]Department of Geography, Norwegian University of Science and Technology, Trondheim, Norway

[7]Department of Physical Geography, Bolin Centre of Climate Research, Stockholm University, Stockholm, Sweden

[8]Institute of Biology of Komi, SC RAS, Syktyvkar, Russia

[9]Department of Earth and Ecosystem Science, Geobiosphere Centre, Geocentrum II, Lund University, Lund, Sweden

[10]Department for Arctic and Climate, Danish Meteorological Institute, Copenhagen Ø, Denmark

[11]Geophysical Institute, University of Alaska Fairbanks, Fairbanks, Alaska

[12]Earth Cryosphere Institute, Tyumen Science Centre, SB RAS, Tyumen, Russia

[13]Department of Geocryological Mapping, GIS, Moscow, Russia

Correspondence
Claire C. Treat, Biogeochemistry Research Group, Department of Biological and Environmental Sciences, University of Eastern Finland, Kuopio, Finland.
Emails: claire.treat@uef.fi, claire.treat@unh.edu

Funding information
Sixth Framework Programme, Grant/Award Number: CARBO-North #036993; National Aeronautics and Space Administration, Grant/Award Number: Arctic Boreal Vulnerability Experiment (ABoVE), NASA-NNX09AI26G; State of Alaska; Itä-Suomen Yliopisto; FP7 Environment, Grant/Award Number: PAGE 21, #282700; Nordic Center of Excellence, Grant/Award Number: DEFROST; Polar Knowledge Canada Science and Technology Program, Grant/Award Number: Project 186; U.S. Department of Energy, Grant/Award Number: DE-FG02-08ER64599; Biotieteiden ja Ympäristön Tutkimuksen Toimikunta, Grant/Award

Abstract

Across the Arctic, the net ecosystem carbon (C) balance of tundra ecosystems is highly uncertain due to substantial temporal variability of C fluxes and to landscape heterogeneity. We modeled both carbon dioxide (CO_2) and methane (CH_4) fluxes for the dominant land cover types in a ~100-km² sub-Arctic tundra region in northeast European Russia for the period of 2006–2015 using process-based biogeochemical models. Modeled net annual CO_2 fluxes ranged from −300 g C m⁻² year⁻¹ [net uptake] in a willow fen to 3 g C m⁻² year⁻¹ [net source] in dry lichen tundra. Modeled annual CH_4 emissions ranged from −0.2 to 22.3 g C m⁻² year⁻¹ at a peat plateau site and a willow fen site, respectively. Interannual variability over the decade was relatively small (20%–25%) in comparison with variability among the land cover types (150%). Using high-resolution land cover classification, the region was a net sink of atmospheric CO_2 across most land cover types but a net source of CH_4 to the atmosphere due to high emissions from permafrost-free fens. Using a lower resolution for land cover classification resulted in a 20%–65% underestimation of regional CH_4 flux relative to high-resolution classification and smaller (10%) overestimation of

regional CO_2 uptake due to the underestimation of wetland area by 60%. The relative fraction of uplands versus wetlands was key to determining the net regional C balance at this and other Arctic tundra sites because wetlands were hot spots for C cycling in Arctic tundra ecosystems.

KEYWORDS

ecosystem modeling, methane, net ecosystem CO_2 exchange, peatland, permafrost, regional carbon balance, Russia, Tundra

1 | INTRODUCTION

The Arctic is warming at a faster rate than the global average (Hartmann et al., 2013). Currently, the Arctic tundra region is generally a net sink of atmospheric CO_2 but a net source of methane (CH_4; McGuire et al., 2012), another potent greenhouse gas (Myhre, Shindell, & Bréon, 2013). However, warmer temperatures in the future may result in the switch of tundra from a net carbon (C) sink to a net C source if soil C losses exceed increase in C uptake by vegetation (Koven et al., 2011). However, the current net sign or magnitude of the combined ecosystem C balance ($CO_2 + CH_4$) in tundra is not well known, especially at regional scales (100–10,000 km^2). Regional C budgets that include both CO_2 and CH_4 have been estimated for Barrow, Alaska (Sturtevant & Oechel, 2013), and Lake Tornetrask in Northern Sweden (Christensen et al., 2007). CO_2 budgets have been calculated for more regions, including Kuparuk River Basin in Alaska (Oechel et al., 2000; Vourlitis et al., 2003), the Barrow experimental observatory (Alaska; Zulueta, Oechel, Loescher, Lawrence, & Paw, 2011), Imnavait Creek and Arctic Alaska (Euskirchen, Bret-Harte, Shaver, Edgar, & Romanovsky, 2017), and Seida (northeast European Russia; Marushchak et al., 2013). Regional CH_4 budgets have been separately calculated for some of the same areas (Christensen et al., 2004; Marushchak et al., 2016; Reeburgh et al., 1998), the Lena River Delta in Siberia (Schneider, Grosse, & Wagner, 2009; Zhang, Sachs, Li, & Boike, 2012), the Yukon–Kuskokwim Delta in Alaska (Bartlett, Crill, Sass, Harriss, & Dise, 1992), and northeast Greenland (Jorgensen, Johansen, Westergaard-Nielsen, & Elberling, 2015). Combining simultaneous estimates of both CO_2 and CH_4 for the same region at the same time is critical for estimating the net C balance of the circum-Arctic because both CO_2 and CH_4 play a substantial role in net C emissions (McGuire et al., 2012; Zhuang et al., 2015) and C emissions may be highly variable across the landscape and over time.

Accurate measurements of present-day regional C balance, including CO_2 and CH_4 exchange, are necessary to detect future changes in C balance, but must properly address the major sources of variability in C cycling: interannual variability and landscape heterogeneity. Interannual climatic variability results in high variability in tundra ecosystem CO_2 exchange and can result in the ecosystem switching from a net C sink to a net C source (Griffis, Rouse, & Waddington, 2000; Heikkinen et al., 2004; Lafleur & Humphreys, 2007; Lafleur, Griffis, &

Rouse, 2001; Oberbauer et al., 2007). Thus, multiple years of measurements are needed to overcome any bias caused by short-term natural climatic variability. Climatic variability also affects CH_4 fluxes: Elevated atmospheric concentrations of CH_4 were observed in northern high latitudes during the wet and warm year of 2007, presumably caused by favorable environmental conditions that promoted CH_4 emissions from wetlands and tundra ecosystems (Bruhwiler et al., 2014). Additionally, episodic fluxes can dominate annual ecosystem CH_4 emissions but can occur infrequently (Mastepanov et al., 2008, 2013), increasing the apparent interannual variability. Without multiple years of measurements, annual CH_4 emissions may be over- or underestimated relative to the long-term mean, depending on the time of sampling (Mastepanov et al., 2013).

Landscape heterogeneity is a driver of the regional C balance in tundra ecosystems (Zulueta et al., 2011), in part because the vegetation composition, productivity, soil type, soil C storage, and permafrost conditions differ greatly within small areas (Hugelius, Routh, Kuhry, & Crill, 2012; Virtanen & Ek, 2014). Within Arctic tundra, lakes and wetlands are hot spots for C cycling. Lakes tend to be hot spots for net CO_2 and CH_4 emissions (Sturtevant & Oechel, 2013), which are derived from the decomposition of autochthonous C, the decomposition of terrestrially derived organic matter, and the lateral flow of dissolved gases including CO_2 and CH_4 (Cole et al., 2007; Kling, Kipphut, & Miller, 1991). Tundra wetlands, such as fens and willow stands, are usually strong C sinks (Marushchak et al., 2013) but also release large quantities of CH_4 as a result of anaerobic decomposition in the water-logged sediments (Bartlett et al., 1992; Marushchak et al., 2016). Near Barrow, Alaska, the CO_2 and CH_4 released from lakes and wetlands, although limited in spatial extent, nearly offset the net C uptake measured in the upland tundra and resulted in a near-neutral regional C balance (Sturtevant & Oechel, 2013). On the other hand, despite hot spots of wetland CH_4 emissions from a tundra site in northeast Greenland, small rates of CH_4 uptake in the large areas of adjacent, well-drained, upland sites resulted in a net regional CH_4 sink rather than net regional source (Jorgensen et al., 2015). These findings highlight the importance of considering hot spots for C cycling together with the ecosystem types that cover larger areas even given low fluxes per unit area.

Accurately capturing the landscape heterogeneity that controls regional C balance requires relatively fine spatial resolution and an

appropriate thematic resolution, meaning representation of land cover types with distinct C dynamics. The spatial resolution must be high enough to detect hot spots for C cycling, such as lakes and wetlands, within the landscape (Bartsch, Höfler, Kroisleitner, & Trofaier, 2016; Davidson et al., 2017; Virtanen & Ek, 2014), which can change greatly depending on the spatial resolution of classification (Muster, Heim, Abnizova, & Boike, 2013). Capturing functional differences among ecosystem types requires a sufficient thematic resolution in landscape classification but must be distinctly and reliably identified using classification techniques. Increasing spatial and thematic resolution can significantly change the regional estimates of C balance (Jorgensen et al., 2015; Schneider et al., 2009; Vourlitis et al., 2003), largely due to the better quantification of emissions hot spots.

The goal of this study was to provide a decadal mean regional CO_2 and CH_4 balance and to characterize the uncertainty due to interannual variability and landscape heterogeneity on the regional CO_2 and CH_4 exchange for a well-characterized site, Seida, in Western Russia. Landscape heterogeneity at Seida is high, with several potential hot spots for C cycling, including upland tundra heath, permafrost peat plateaus, permafrost-free fens, and lakes located within 200 m^2. We used process-based biogeochemical models that were calibrated and validated with independent CO_2 and CH_4 flux measurements (Marushchak et al., 2016, 2013 ; Voigt et al., 2017) to estimate CO_2 and CH_4 fluxes between the dominant regional land cover types and the atmosphere. These estimates provide an important addition to high-latitude regional C budgets by addressing an existing spatial data gap at the tundra–taiga interface in the discontinuous permafrost zone in northwestern Russia.

2 | MATERIALS AND METHODS

2.1 | Site description and classification

The study site, Seida, is located in the northern forest–tundra subzone with discontinuous permafrost, near the Seida settlement in northeast European Russia (67°03′N, 62°56′E; Figure 1). At Vorkuta climate station (67°48′N, 64°10′; Figure 1), 70 km to the northeast of Seida, the mean average annual air temperature for 1977–2006 was −5.6°C and the mean annual precipitation was 501 mm (Komi Republican Centre for Hydrometeorological and Environmental Monitoring).

The regional landscape at Seida was divided into three major land cover types using land cover classification methods: upland tundra (58%), permafrost peat plateaus (24%), and low-lying, permafrost-free fens (14%; Table 1). Within these major land cover types, several land cover subtypes were identified based on the dominant vegetation (Supporting information Figure S1 in
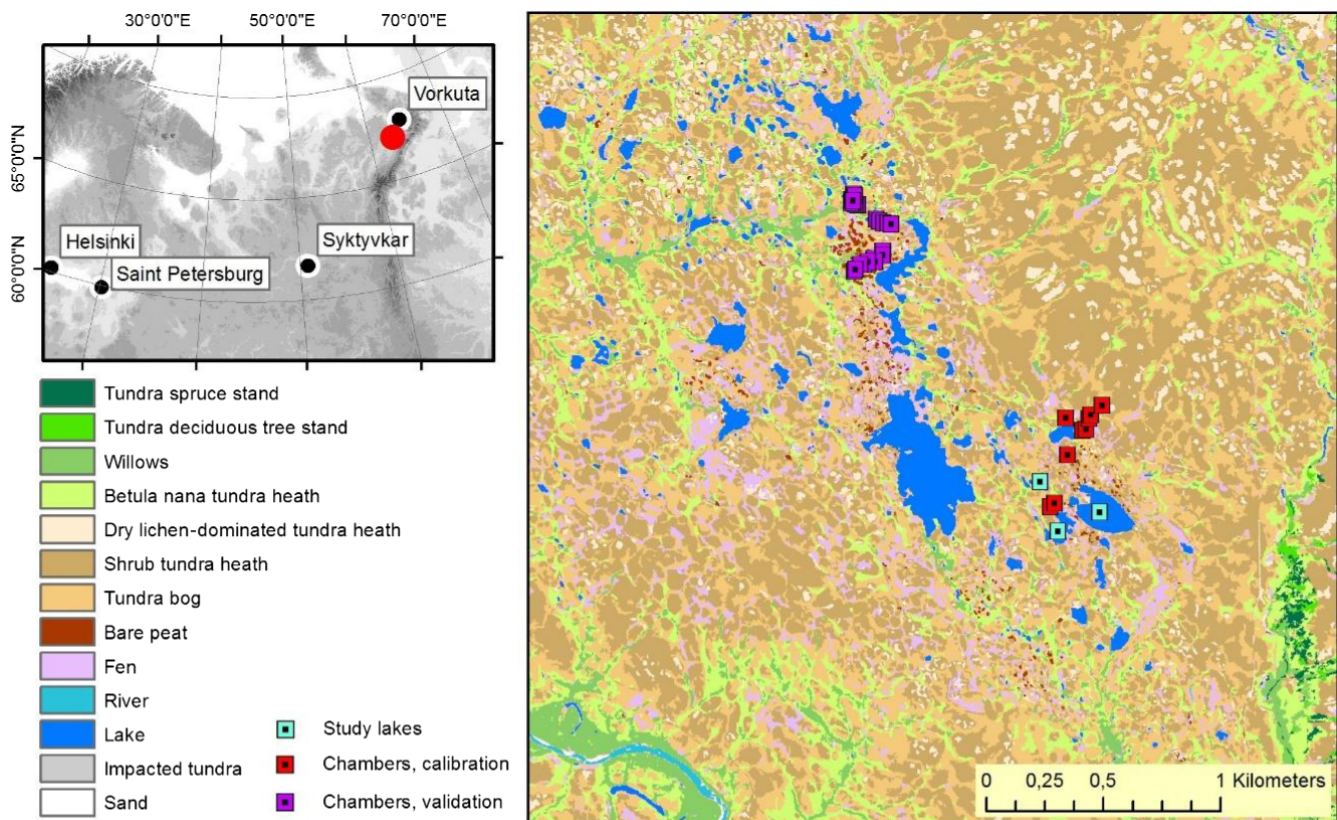

FIGURE 1 Map of the Seida study region. Top left: Location of Seida study region (red circle). Right: land cover classification and the locations of the flux measurement sites within the Seida study region. Squares indicate sites used in the NEST-DNDC model calibration (red; 2007–2008), NEST-DNDC model validation (purple; 2012–2013), and ALBM model validation (aqua)

TABLE 1 Major land cover types, spatial coverage, and mean modeled CO_2 and CH_4 fluxes for 2006–2015

Major land cover type	Land cover subtypes (LCT)	Area (%)	GPP (g C m^{-2} year^{-1}) F_{Plot} (SE)	ER (g C m^{-2} year^{-1}) F_{Plot} (SE)	NEE (g C m^{-2} year^{-1})		CH$_4$ (g C m^{-2} year^{-1})	
					F_{Plot} (SE)	$F_{Regional}$ (SE)	F_{Plot} (SE)	$F_{Regional}$ (SE)
Tundra heath	Moist shrub	20.2	270 (17)	220 (5)	−60 (13)	−12 (2.6)	−0.1 (0.0)	0.0 (0.0)
	Dry shrub	15.4	170 (11)	160 (6)	−6.4 (5.2)	−1.0 (0.8)	0.1 (0.0)	0.0 (0.0)
	Dwarf birch	15.2	280 (16)	200 (5)	−74 (11)	−11 (1.7)	−0.1 (0.0)	0.0 (0.0)
	Dry lichen	7.1	130 (7)	130 (4)	2.7 (4.1)	0.2 (0.3)	0.0 (0.0)	0.0 (0.0)
Peat plateau	Dry tundra bog	8.3	260 (11)	180 (4)	−78 (7.9)	−6.6 (0.7)	0.0 (0.0)	0.0 (0.0)
	Moist tundra bog	15.0	340 (15)	250 (5)	−83 (11)	−13 (1.7)	−0.2 (0.0)	0.0 (0.0)
Fen	Willow fen	8.7	840 (41)	540 (66)	−300 (30)	−26 (2.6)	22.3 (2.1)	2.0 (0.2)
	Carex fen	5.1	480 (19)	380 (49)	−99 (33)	−5.1 (1.7)	21.0 (1.9)	1.1 (0.1)
	Eriophorum fen	0.6	110 (4)	82 (12)	−29 (9.6)	−0.2 (0.1)	17.2 (1.5)	0.1 (0.0)
Other	Forest	2.3	250 (12)	220 (9)	−25 (5.5)	−0.6 (0.1)		
	Lakes	1.1			10 (0.4)	0.1 (0.0)	0.3 (0.0)	0.0 (0.0)

Notes. Values in parentheses indicate the standard error (SE) of the land cover type due to interannual variability over the 10 years (n = 10). CO_2 fluxes: gross primary productivity (GPP), ecosystem respiration (ER = Rh + R_a), net ecosystem CO_2 exchange (NEE), and CH_4 flux. Plot-scale flux measurements (F_{Plot}) represent the measured flux within each land cover type, while spatially weighted fluxes ($F_{Regional}$) represent the contribution of each LCT to the regional flux ($F_{Regional, LCT} = F_{Plot, LCT} \times Area_{LCT}/Area_{tot}$). Positive fluxes indicate release to the atmosphere. Total area of the study region was 98.6 km^2.

Appendix S1). In this region, vegetation composition corresponds to factors such as water table position, organic soil thickness, and pH, which are related to local topography and drainage (Hugelius et al., 2011), as is common in many northern landscapes (Bubier, Moore, & Crosby, 2006). The land cover classification was derived from a QuickBird satellite image (2.4 m pixel size) covering 98.6 km^2 around the flux measurement site, acquired on July 6, 2007 (QuickBird© 2007, DigitalGlobe). Classifications were produced using an object-based classification with multiresolution segmentation. Classification accuracy was tested with field-collected verification data. This approach also differs from broader land cover classifications made at the circum-Arctic scale (Walker et al., 2005), which do not capture much of the fine-scale landscape heterogeneity associated with local conditions. To assess the effect of reduced spatial resolution, the land cover classification was resampled to 20, 160, 320, and 1,280 m resolution by calculating majority land cover class in each pixel (Figure 2). Further detail on the soil, vegetation, and classification schemes can be found in Marushchak et al. (2011, 2013) and Hugelius et al. (2011).

The upland tundra, common throughout the study region, is developed on silty to sandy well-drained soils overlain by variable, but relatively thin surface organic horizons (<20 cm). The upland soil is covered with shrub tundra vegetation dominated by *Betula nana*, numerous *Salix* sp. (including *Salix phylicifolia* and *Salix glauca* in wetter areas and dwarf willows such as *Salix reticulata, Salix arctica*, and *Salix polaris* in dry areas), and dwarf shrubs, such as *Vaccinium uliginosum* and *Vaccinium vitis-idaea*. Four dominant vegetation types were identified: dry shrub tundra heath, moist shrub tundra heath, dwarf birch tundra heath, and dry lichen tundra heath that was found primarily on ridgetops.

The permafrost peat plateaus consist of variable, but often deep (up to 4 m), organic deposits whose surfaces are elevated above other peatlands due to frost heave from the accumulation of massive

ground ice. We used two land cover subtypes to represent the dry and moist bog vegetation types found on the peat plateaus. The dry peat plateau subtype is well-drained and has *Ledum decumbens* and *Rubus chamaemorus* as dominant vascular plants, mosses (e.g., *Dicranum* spp.) and lichens (e.g., *Cladina* spp.) in the ground layer. The moist peat plateau subtype occurs in wet *Sphagnum* depressions with *R. chamaemorus* and *V. uliginosum*.

Permafrost-free fens and willow stands are located in low-lying parts of the landscape, often adjacent to the peat plateaus, and are dominated by graminoids (*Carex* spp., *Eriophorum* spp.), or willows (*Salix* spp.). In the fens, there is a floating *Sphagnum* mat and the water table is near the surface throughout the growing season. The dominant vascular plant types in fens were sedges (*Carex aquatilis*) and cotton grasses (*Eriophorum russeolum*). Willow, including *Salix phylicifolia and S. lapponum*, was the other type of dominant vegetation in fens, occurring in 50–120 cm high stands in low-lying areas with peaty soils.

In addition to upland tundra and peatlands, thermokarst lakes are interspersed throughout the peat plateaus and cover 1.1% of the study area. Deciduous and spruce forests are scattered across the broader Seida region, covering 2.3% of the study area, but do not occur within the calibration and validation study areas.

2.2 | Ecosystem modeling

We used the process-based model, NEST-DNDC (Zhang et al., 2012) to simulate C fluxes from the dominant regional land cover types: upland tundra, peat plateaus, and permafrost-free fens. Two additional, independent models simulated C fluxes from the forest and lake components of the Seida landscape. Modeling of the forested land cover type used LPJ-GUESS (Lund-Potsdam-Jena General Ecosystem Simulator, Smith, Prentice, & Sykes, 2001), and modeling of the lakes was done using the Arctic Lake Biogeochemistry
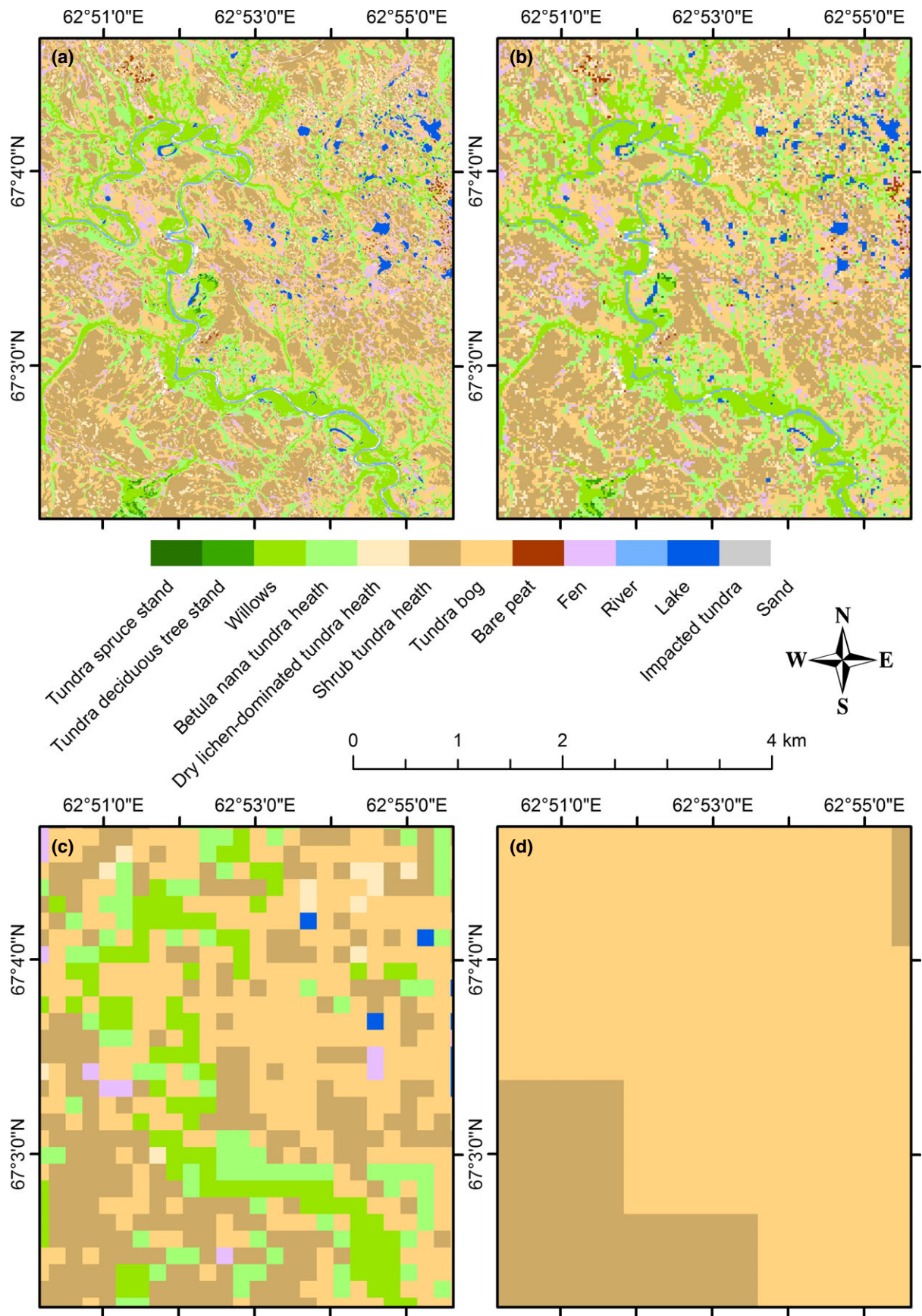
FIGURE 2 Land cover classification for Seida derived from the same original image using different resolutions: (a) original Quickbird 2.4 m resolution image; (b) 20 m resolution; (c) 160 m resolution; (d) 1,280 m resolution

model (ALBM; Tan et al., 2017; Tan, Zhuang, & Walter Anthony, 2015).

2.2.1 | Modeling of upland tundra, permafrost peat plateaus, and permafrost-free fens

We used the NEST-DNDC to model water table level, active layer thickness, and C fluxes for upland tundra heath, peat plateaus, and permafrost-free fens. NEST-DNDC is a process-based model that integrates an existing biogeochemical model DeNitrification-DeComposition (DNDC; Li, Aber, Stange, Butterbach-Bahl, & Papen, 2000) with a permafrost model Northern Ecosystem Soil Temperature (NEST; Zhang, Chen, & Cihlar, 2003) and is capable of simulating an ecosystem domain consisting of a number of plant communities (Zhang et al., 2012). NEST-DNDC models rates of ecosystem respiration (ER = Rh + R_a), gross primary productivity (GPP), net ecosystem CO_2 exchange (NEE = GPP − ER), and CH_4 fluxes, including vegetation transport and ebullition emission pathways. Previously, NEST-DNDC has been tested against observations of CH_4 fluxes measured by closed chambers and eddy covariance (EC) method in a polygonal permafrost area in the Lena River Delta, Russia (Zhang et al., 2012). We used a synthetic climate driver dataset for the period of 2006–2015 (Figure 3). The climate drivers were derived from a combination of site measurements (2006–2011) and bias-corrected observations for 2012–2015 from nearby Vorkuta (~70 km NE, 67°30′N, 64°2′E) and Salekhard (66.5294°N, 66.5294°E) meteorological stations (NOAA National Centers for Environmental Information, https://www.ncdc.noaa.gov/, 2012–2015). Additional detailed information about model parameterizations and evaluation can be found in Supporting information Appendix S1.

2.2.2 | Forest ecosystem modeling

We used the Arctic-enabled LPJ-GUESS to simulate forest ecosystem C dynamics for the Seida region. This model has been specifically developed to simulate treeline and shrub expansion in tundra ecosystems and has been validated for high-latitude regions in this region (Miller & Smith, 2012; Zhang et al., 2013), while the NEST-DNDC model used for nonforested land cover types could not be parameterized for forest stands in this region due to lack of field measurements in this ecosystem type. For this study, LPJ-GUESS (Smith et al., 2001) was modified to model upland, high-latitude ecosystems by incorporating recent developments to LPJ-DGVM that include improved determination of soil temperatures and soil freezing processes using a four-layer soil column and a snowpack (Wania, Ross, & Prentice, 2009, 2010; Wolf, Callaghan, & Larson, 2008). The Arctic-enabled LPJ-GUESS has an expanded set of plant function types (PFTs) for use in high-latitude upland regions. Thirteen PFTs were simulated in this study, including five tree types, evergreen and deciduous short shrubs (up to 0.5 m in height), evergreen and deciduous tall shrubs (up to 2 m in height), and four open ground, herbaceous
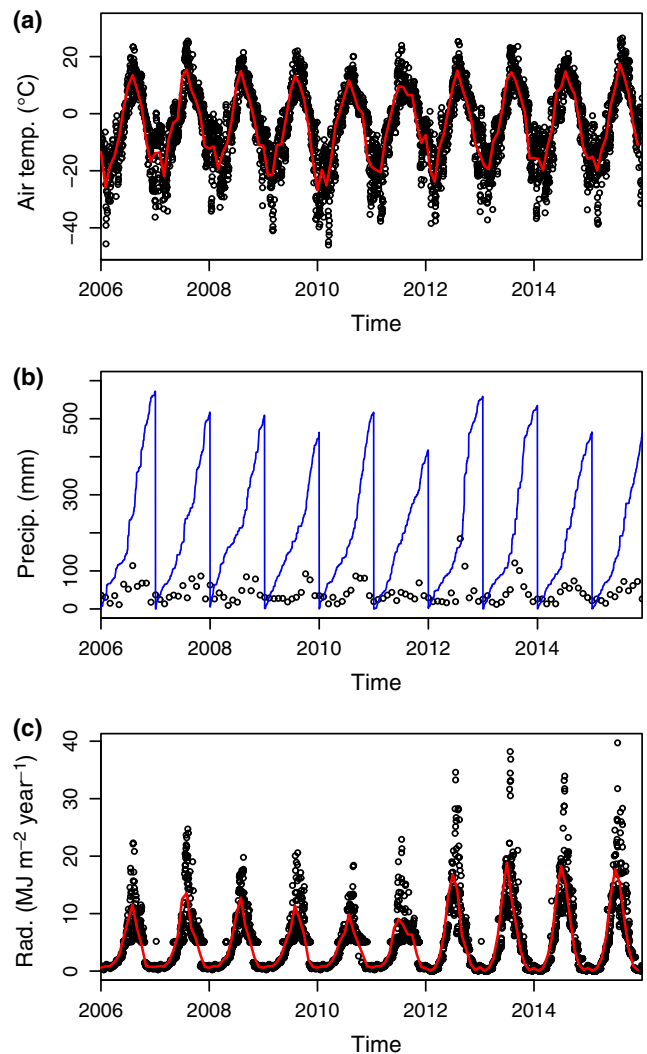

FIGURE 3 Climate driver data for Seida for January 1, 2006, to December 31, 2015. (a) mean daily air temperature (circles) and mean monthly air temperature (line); (b) total monthly precipitation (circles) and cumulative annual precipitation (line); (c) daily incoming solar radiation (circles) and mean monthly incoming solar radiation (line)

types (Wolf et al., 2008). The C balance simulated by the Arctic-enabled LPJ-GUESS used here is in broad agreement with other, similar bottom-up process-based models, inverse models, and upscaled site-based observations (McGuire et al., 2012). Additional information on model parameterization can be found in Supporting information Appendix S1.

2.2.3 | Lake ecosystem modeling

The Arctic Lake Biogeochemistry Model (ALBM) is a one-dimensional process-based climate-sensitive lake biogeochemistry model that simulates CO_2 and CH_4 emissions from Arctic lakes (Tan et al., 2017, 2015). Carbon dioxide and CH_4 emissions from Arctic lakes are determined by their surface concentrations and transfer velocities.

To estimate surface CO_2 concentrations, the ALBM model simulates the processes of photosynthesis, the mineralization and deposition of organic matter, and the loading of organic and inorganic C through water flow and permafrost thawing within a one-dimensional sediment and water column (Tan et al., 2017). In the model, photosynthesis rates are controlled by the levels of photosynthetically active radiation, temperature, phosphorus, and chlorophyll a. Mineralization of organic matter is represented in two pathways: microbial and photochemical degradation. To estimate surface CH_4 concentrations, the ALBM model simulates CH_4 production, oxidation, and transport (both diffusion and ebullition) within a one-dimensional sediment and water column (Tan et al., 2015). Methane production occurs in both surface and deep sediments. The transfer velocities of CO_2 and CH_4 at the water–air interface are modeled as a function of wind speed, water mixing depth, and gas Schmidt number (Tan et al., 2017). The climate drivers for ALBM were the same as for NEST-DNDC (Section 2.1.1).

2.3 | Measurements for model calibration and verification

DNDC and ALBM were calibrated and validated against independent field measurements from the Seida region (Supporting information Appendix S1). Soil temperature, water table, and seasonal thaw depth were measured during field campaigns in 2007–2008. Snow depths were measured during the winter of 2007–2008. For C fluxes in DNDC, CO_2 and CH_4 exchange rates were measured in all the vegetation subtypes on peat plateaus, fens, and uplands using a static chamber technique throughout the growing seasons in 2007, 2008, 2012, and 2013 and during the winter of 2007–2008 (Marushchak et al., 2016, 2013 ; Voigt et al., 2017). Gross primary productivity was calculated as the difference between NEE using transparent chambers and ER, measured using opaque chambers. Observed daily CO_2 flux measurements were interpolated from the instantaneous chamber measurements using empirical relationships with PAR, LAI, soil temperature, soil moisture, and water table for each measurement location (Marushchak et al., 2013, Voigt et al., 2017 [Tables S5, S6]). Interpolating the observations to daily values from instantaneous observations reduced bias in CO_2 flux measurements due to diurnal variation in PAR and soil temperatures; diurnal variability in CH_4 fluxes was assumed to be small at this site. The annual measurements from 2007 to 2008 were used for model calibration, whereas growing season measurements from 2012 to 2013 at a subsite roughly 2 km northwest were used for verification purposes (Figure 1). We tested for model bias using linear regressions between interpolated measurements and model output using R (R Development Core Team, 2008) and report the results in Supporting information Appendix S1.

The ALBM model was calibrated and validated at the Seida site using the measured CO_2 and CH_4 fluxes from three Seida lakes during the open water period of 2007 and 2008 (Repo et al., 2007). Details on specific calibration and validation methods are described in Tan et al. (2015, 2017).

2.4 | Regional C balance and C feedback

We estimated the regional C balance from Seida using a simple upscaling approach using the areas of each land cover type within the study region (Marushchak et al., 2013; Oechel et al., 2000; Reeburgh et al., 1998) and the modeled decadal fluxes for each land cover type. We determined the gaseous net C exchange (CO_2-C + CH_4-C) and mean areal emissions for each land cover type. Using the mean areal emission allows a comparison of the contribution of each land cover type to the regional C balance. To determine the mean areal emissions (mean spatially weighted emission) for each land cover type (LCT), we used the equation:

$$F_{\text{regional}-\text{LCT}} = A_{\text{LCT}} \times F_{\text{plot}-\text{LCT}}/A_{\text{total}} \tag{1}$$

where $F_{\text{regional-LCT}}$ is the mean areal emission of each land cover type normalized over the study domain, A_{LCT} is the area of each land cover type, $F_{\text{plot-LCT}}$ is the modeled CO_2 or CH_4 flux that is comparable to the plot-scale measurements, and A_{total} is the total area of the Seida study region (98.6 km^2).

We compared the variability in CO_2 and CH_4 emissions among land cover classifications and years using the coefficient of variation, calculated as the standard deviation/mean, given as a percent. This normalized metric allows the comparison of variability among samples.

3 | RESULTS

3.1 | C fluxes during calibration (2007–2008) and validation (2012–2013) periods

In upland tundra heath vegetation types, NEST-DNDC simulated the magnitude and daily variation of CO_2 fluxes well during the calibration period of 2007–2008 (Figure 4a–c) and the validation period at nearby Seida II in 2012–2013 (Figure 4e–g). In tundra heath, both modeled and measured CH_4 fluxes were generally quite small (<5 mg C m^{-2} day^{-1}; Figure 4d,h), with noticeable CH_4 emission peaks during the spring and fall periods due to ebullition events likely associated with soil freeze and thaw. Model output at the peat plateau site matched well with the daily interpolated flux chamber measurements during the calibration period of 2007–2008 for NEE, ER, and GPP (Figure 5a–c) and during the validation period of 2012–2013 (Figure 5g), although the model had some difficulty capturing high rates of ER during the spring and early summer. The peat plateaus were net sinks of CH_4 in the model (–0.1 g C m^{-2} year^{-1}; Figure 5d), whereas measurements showed fluxes of 0.2 ± 0.2 g C m^{-2} year^{-1} (Marushchak et al., 2016); a similar trend occurred in 2012–2013 (Figure 5h). The model also simulated noticeable CH_4 emission peaks in the peat plateaus during the spring and fall due to episodic emissions associated with soil freeze and thaw. Modeled growing season soil temperatures depth were cooler than the observations, resulting in a shallower seasonal thaw depth than observations, particularly for tundra heath and peat plateau vegetation types (Supporting information Appendix S1).
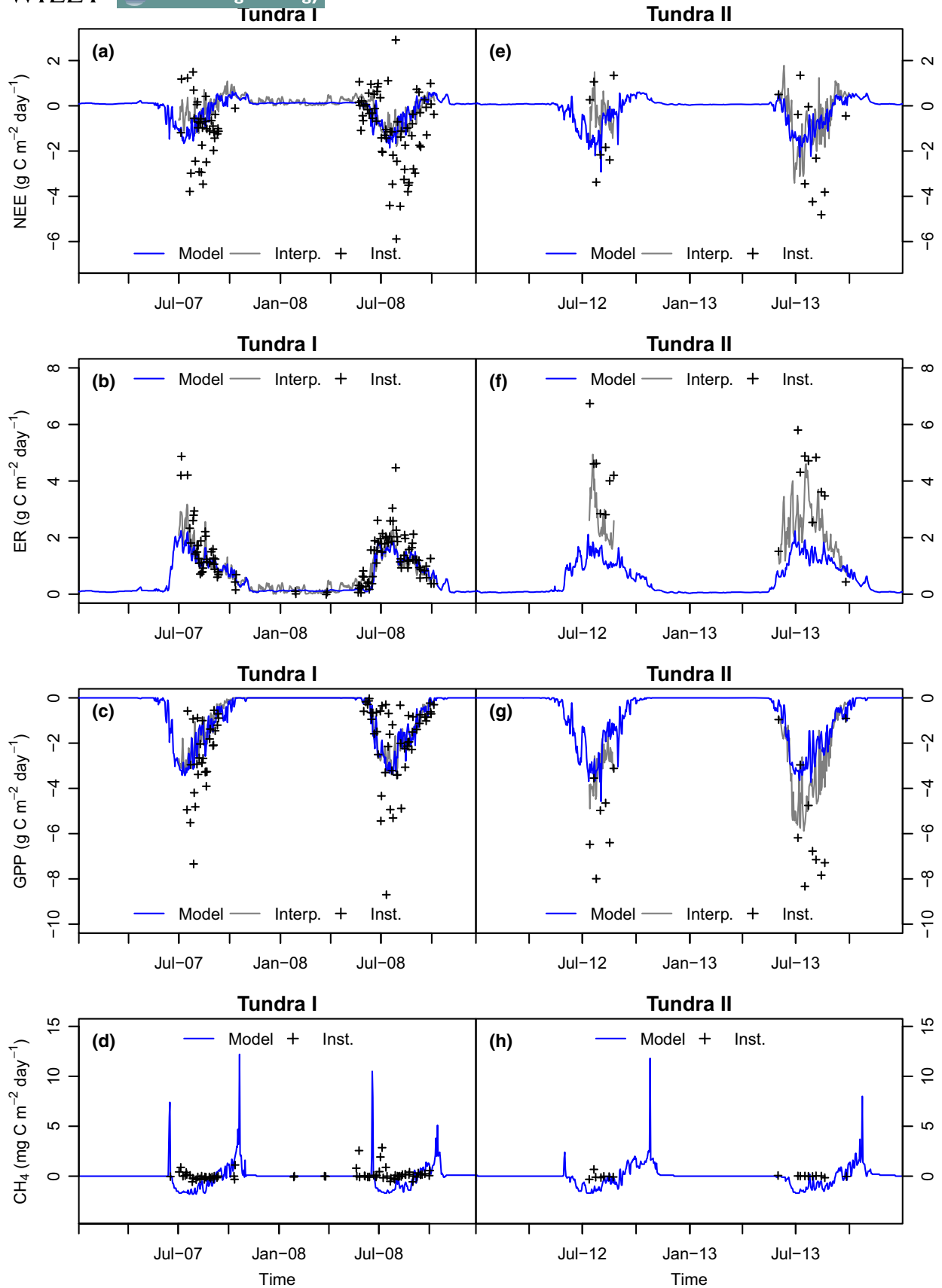
FIGURE 4 Modeled and measured CO_2 and CH_4 flux data for calibration period of 2007–2008 (left panels) and validation period of 2012–2013 (right panels) for the tundra heath land cover types at Seida. Model results are shown by blue solid line, mean daily interpolated fluxes (Interp.) are shown by gray solid line, and instantaneous chamber measurements (Inst.) are shown by black crosses [Colour figure can be viewed at wileyonlinelibrary.com]
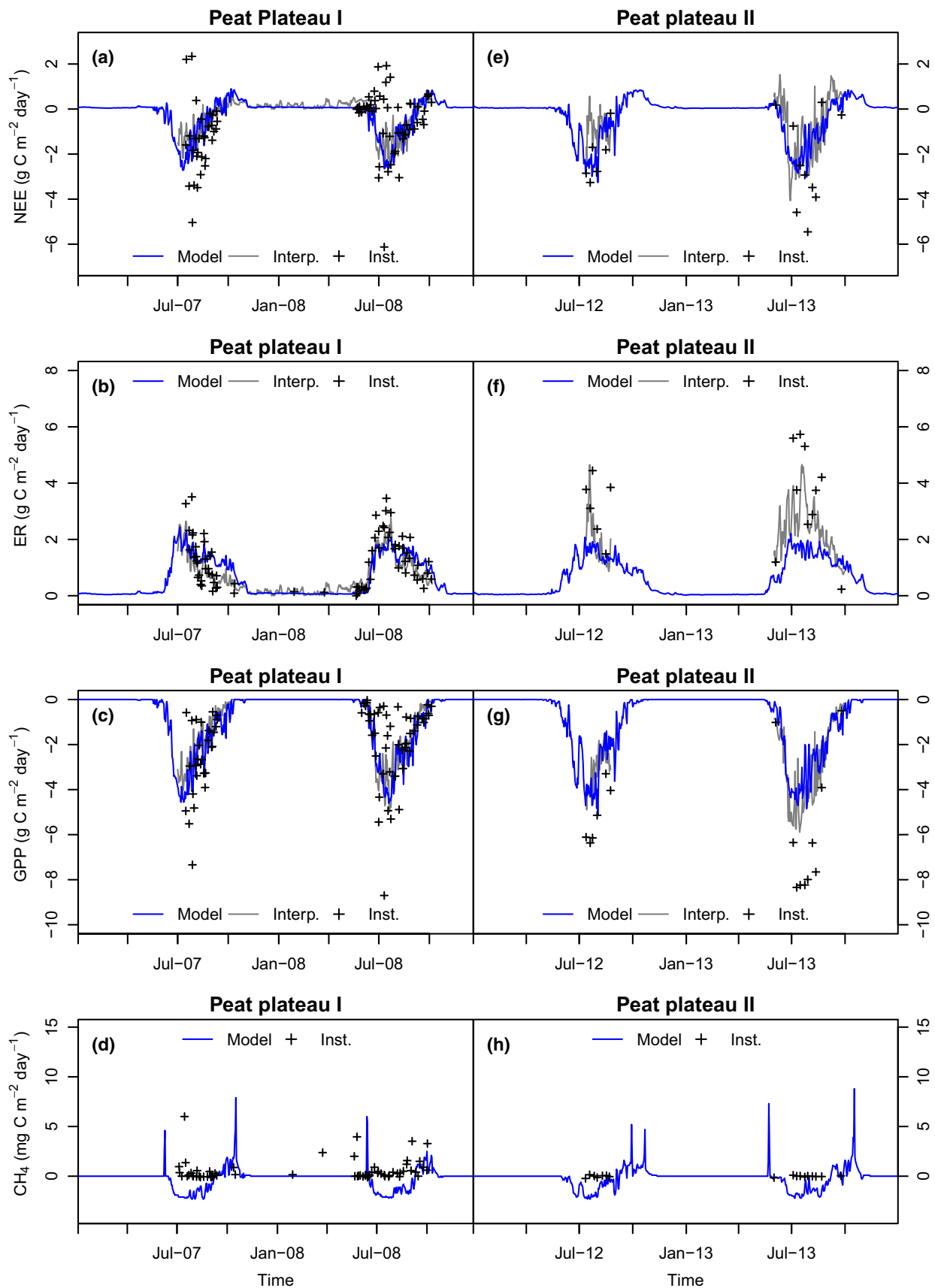
FIGURE 5 Modeled and measured CO_2 and CH_4 flux data for calibration period of 2007–2008 (left panels) and validation period of 2012–2013 (right panels) in the Seida peat plateaus. Model results are shown by blue solid line, mean daily interpolated fluxes (Interp.) are shown by gray solid line, and instantaneous chamber measurements (Inst.) are shown by black crosses [Colour figure can be viewed at wileyonlinelibrary.com]
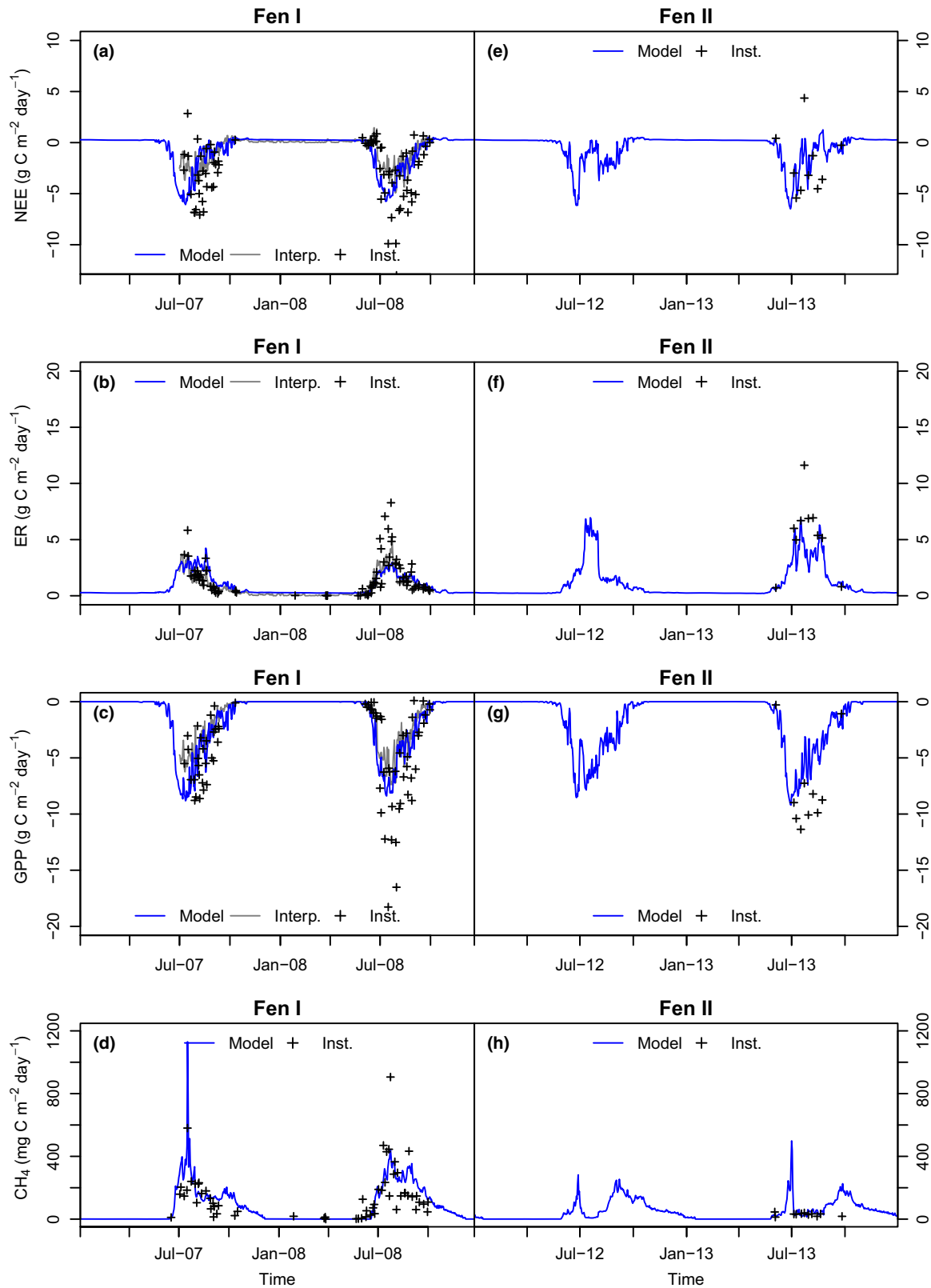
FIGURE 6 Modeled and measured CO_2 and CH_4 flux data for calibration period of 2007–2008 (left panels) and validation period of 2012–2013 (right panels) for the permafrost-free fen land cover types at Seida. Fen II was not measured in 2012. Model results are shown by blue solid line, mean daily interpolated fluxes (Interp.) are shown by gray solid line, and instantaneous chamber measurements (Inst.) are shown by black crosses [Colour figure can be viewed at wileyonlinelibrary.com]
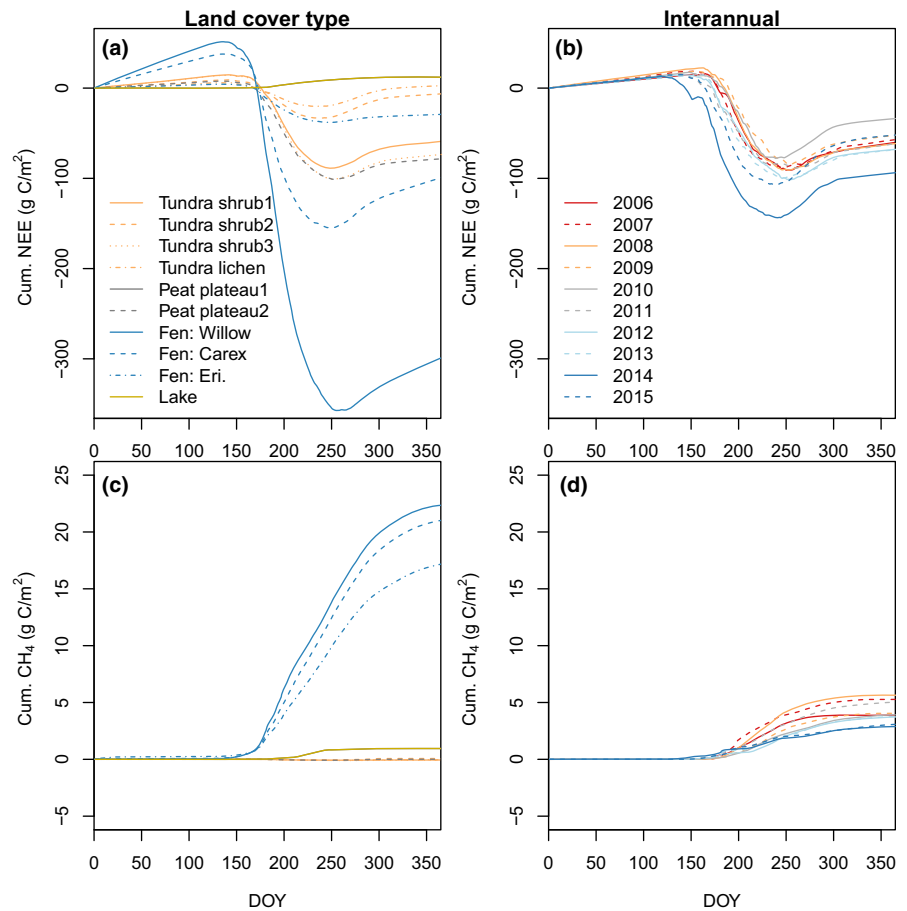
FIGURE 7 Modeled variability among land cover classes (left) and years (right) of cumulative NEE and CH_4 flux for 2006–2015. (a) Variability in the cumulative NEE among the land cover types using the decadal mean daily flux (F_{plot}); (b) Interannual variability in the cumulative NEE over the year for the region using 2.4 m resolution land cover classification ($F_{regional}$); (c) Variability in the cumulative CH_4 flux among the land cover types using the decadal mean daily CH_4 flux (F_{plot}); (d) Interannual variability in the cumulative CH_4 flux over the year for the region using 2.4 m resolution land cover classification ($F_{regional}$)

Agreement between model output and daily fluxes at the fen vegetation types during the calibration period of 2007–2008 and the validation period 2012–2013 was quite good for CO_2 flux components (Figure 6a–c,e–g) and CH_4 flux (Figure 6d,h). The model simulated permafrost in the fen vegetation types in deeper soils (>150 cm), while permafrost was not observed in the field, which is likely related to local hydrologic conditions that affect lateral and vertical heat fluxes (Kurylyk, Hayashi, Quinton, Mckenzie, & Voss, 2016). Further discussion of the model evaluation can be found in Supporting information Appendix S1.

3.2 | Decadal variability among land cover types and years

Modeled CO_2 fluxes averaged over the study period 2006–2015 differed greatly among land cover types, but nearly all land cover types were net sinks of CO_2 (Figure 7a, Table 1). Willow fens showed strong net CO_2 uptake that was approximately three times larger than NEE in other land cover types (Figure 7a). NEE in *Carex* fens, peat plateaus, moist shrub, and dwarf birch tundra heath were all similar in magnitude and ranged from −60 to −100 g C m^{-2} year^{-1}. Both lakes and lichen tundra heath were net sources of CO_2 to the atmosphere, emitting 10 ± 0.4 and 3 ± 4 g C m^{-2} year^{-1}, respectively (Table 1, Figure 7). Both ER and GPP were greatest in the

Willow and *Carex* fen vegetation types and lowest in the *Eriophorum* fen and the lichen heath tundra (Table 1).

Modeled CH_4 emissions ranged from a small net uptake of CH_4 in the dry and upland land cover types to a significant source of CH_4 in the wetlands and a small source in the lakes (Figure 7c, Table 1). Generally, the net CH_4 flux from all the dry vegetation types, including both the vegetation types on the mineral tundra and the permafrost peat plateau bogs, was essentially zero (−0.04 ± 0.02 g C m^{-2} year^{-1}). The vegetation types with highest NEE, Willow and *Carex* fens, also had the largest mean annual CH_4 emissions, which ranged from 17.2 to 22.3 g C m^{-2} year^{-1} (Figure 7a,c, Table 1). Of the three lakes modeled in the Seida region, CH_4 fluxes were the largest from a small thermokarst lake (3.3 ± 0.2 g C m^{-2} year^{-1}) while fluxes for the other two, larger lakes were smaller by an order of magnitude (0.2 – 0.3 g C m^{-2} year^{-1}) due to differences in organic matter inputs for CH_4 production associated with higher productivity and vegetation colonization.

There was significant interannual variability in the modeled regional C fluxes during this decadal period, although all years were net CO_2 sinks. Between 2006 and 2015, NEE ranged from a low of −34 g C m^{-2} year^{-1} in 2010 to a high of −94 g C m^{-2} year^{-1} in 2014 (Figure 7b). Between 2006 and 2015, CH_4 flux ranged from 2.9 g C m^{-2} year^{-1} in 2014 and 2015 to 5.6 g C m^{-2} year^{-1} in 2008 (Figure 7d). For the study region as a whole, the coefficient of

variation (standard deviation/mean) in NEE due to interannual variability was 25%. In comparison, the coefficient of variation of NEE due to differences among land cover types was 150% (Figure 7a,b). The interannual variability of CH_4 (22%) was less than NEE (25%; Figure 7d,b). In comparison, the coefficient of variation of CH_4 flux due to differences among land cover types was 155%.

Additionally, there were differences in the relative range of interannual variability within each land cover type for both modeled NEE and CH_4 flux between 2006 and 2015 (Table 1). The interannual variability of NEE was smallest in lakes (7%), followed by peat plateaus (37%), fens (53%), forest (70%), and tundra heath (76%). The high variability in tundra heath vegetation types was mainly due to high interannual variability in dry lichen tundra heath (490%) and dry shrub tundra heath (260%); these vegetation types were net C sinks in some years (2012–2015) but net C sources in other years (2006–2011). Similarly, *Carex* and *Eriophorum* fens also had relatively high interannual variability (~105%), with net C uptake occurring in most years except 2014 and 2015. The interannual variability in CH_4 flux was smallest in lakes (13%), followed by fens (28%). The interannual variability in CH_4 flux was larger in peat plateau (85%) and tundra vegetation types (105%), which were dry and had little or no CH_4 flux except for small pulse emissions during the spring and fall (Figures 3, and 4). The magnitude of the interannual variability among land cover types did not seem to follow any trends in vegetation or soil moisture (Table 1; Supporting information Table S1 in Appendix S1).

3.3 | Regional-scale C balance

During the study period 2006–2015, the Seida region was modeled to be a mean net CO_2 sink of -75 ± 8 g C m^{-2} year^{-1} when using high-resolution (2.4 m) land cover data (Table 2, Figure 8a). A large part of the net CO_2 uptake, 35%, occurred in the willow fens ($F_{regional}$; Table 1). Moist shrub tundra heath, dwarf birch tundra heath, and moist permafrost bogs were also net sinks of CO_2 on the regional scale but sequestered less than half of the willow fen

TABLE 2 Major land cover types, spatial coverage, and mean (*SE*) modeled regional fluxes ($F_{regional}$), including NEE, and CH_4 flux, for 2006–2015

Major land cover type	Area (%)	NEE (g C m^{-2} year^{-1})	CH_4 (g C m^{-2} year^{-1})
Tundra heath	57.9	−24.2 (3.2)	0.0 (0.0)
Peat plateau	23.3	−19.1 (1.8)	0.0 (0.0)
Fen	14.4	−31.6 (3.1)	3.2 (1.4)
Forest	2.3	−0.6 (0.1)	0.0 (0.0)[a]
Lake	1.1	0.1 (0.0)	0.0 (0.0)
Total	100	−75 (8)	3.1 (0.2)

Notes. Positive fluxes indicate release to the atmosphere. Residual landscape area includes bare peat circles, human-impacted tundra, and sand and represents 1.1% of the regional area; fluxes from this region were assumed to be negligible.

[a]Using median upland forest daily flux of −0.07 g CH_4 m^{-2} day^{-1} from Olefeldt et al. (2013) and assuming 120-day emission season at Seida.
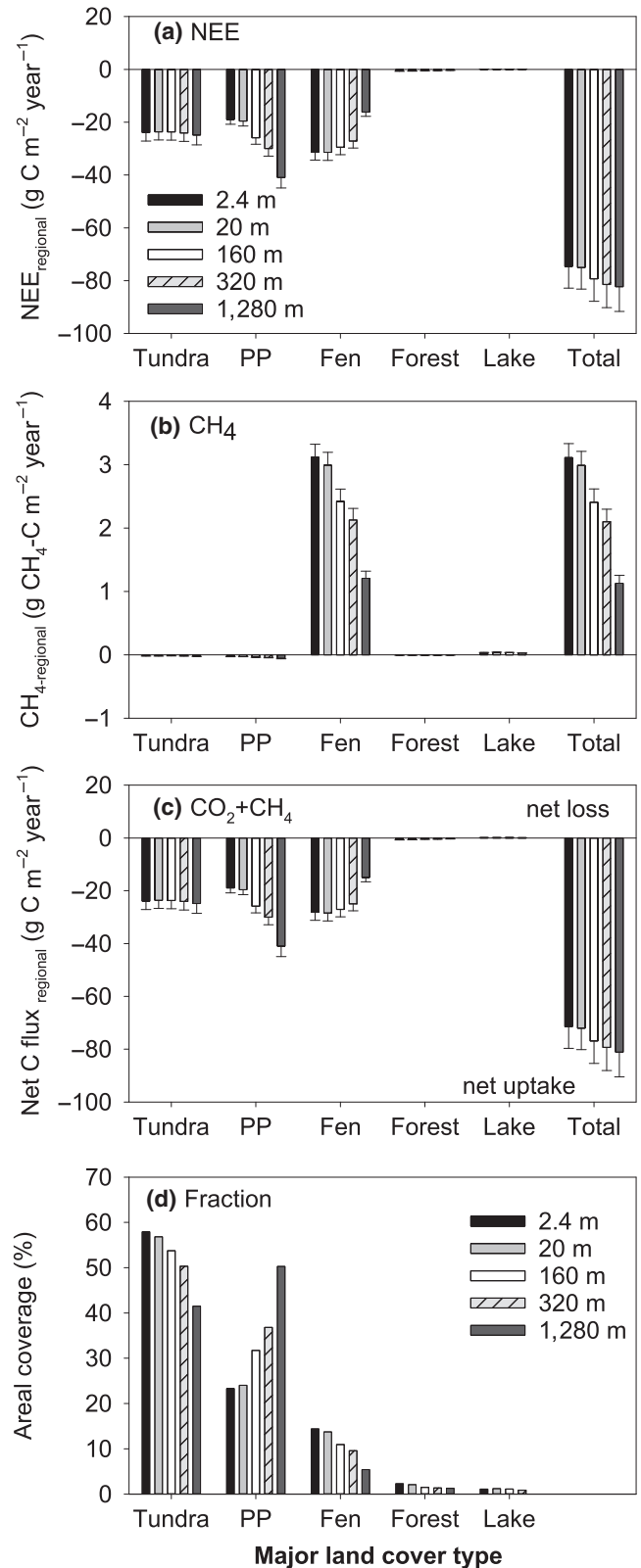

FIGURE 8 Modeled mean areal CO_2 and CH_4 fluxes ($F_{regional}$) during 2006–2015 for major land cover types using different resolutions for land cover classification, ranging from 2.4 m to 1,280 m. Decadal mean modeled (a) NEE, (b) CH_4 emissions, (c) net C exchange ($CO_2 + CH_4$), and (d) areal coverage (%) for the major land cover types in the Seida region for present day at different resolutions (Figure 2)

uptake (Table 1). The region was modeled to be a net CH_4 source to the atmosphere of 3.1 ± 0.3 g C m^{-2} year^{-1} due to the substantial emissions from the willow and *Carex* fens, which together contributed nearly 100% of the regional CH_4 emission. Modeled methane emissions from wetlands were not offset by the small rates of modeled net CH_4 uptake from the dry tundra vegetation types, but this uptake did slightly reduce (<5%) the regional CH_4 emission (Table 1, Figure 8b).

3.4 | Role of spatial landscape heterogeneity

The regional C budget changed considerably when, instead of the highest available 2.4 m pixel resolution, a lower resolution land cover classification was used (Figures 2 and 8). At 20 m resolution, the fraction of each major land cover type was still similar to that from 2.4 m classification (Figure 8d), and subsequently, total regional NEE and CH_4 were similar (within 5%) to the higher resolution (2.4 m) classification (Figure 8a–c). However, at lower resolutions (≥160 m), the fraction of peat plateaus increased at the expense of fen and tundra coverage (Figure 8d, Figure 2), causing a significant decrease in the regional NEE and CH_4 of fens (5%–120%) and a 40%–120% increase in NEE and CH_4 in peat plateaus (Figure 8a–c). Overall, the shift from fens and tundra to peat plateaus using the lower resolution classification increased the total regional CO_2 uptake by <10% (Figure 8a) and decreased total regional CH_4 emissions by 20%–60% (Figure 8b).

4 | DISCUSSION

4.1 | Land cover type versus interannual variability

There have been a limited number of estimates of long-term regional C fluxes from Arctic tundra, and even fewer that combine CO_2 and CH_4 fluxes. This study allowed us to compare the relative effects of variability among years and land cover types on CO_2 and CH_4 emissions in a well-characterized region. The modeled interannual variability of CO_2 and CH_4 fluxes was 20%–25% of the mean fluxes (Figure 7b,d), reflecting a range of climatic conditions from cool and wet in 2010 to warmer with intermediate precipitation in 2014 and 2015 (Figure 3). The interannual variability in fluxes was small, however, compared to the variability associated with land cover types (150%). For example, permafrost-free willow fens had large net CO_2 uptake and high CH_4 emissions, dry lichen tundra heath had near-neutral net CO_2 exchange and CH_4 flux, and lakes were a net source of both CO_2 and CH_4 (Figure 7a,c).

In remote sites like Seida, as well as for much of the Arctic, modeling can be an important tool for estimating net C exchange as extended monitoring of C fluxes is impractical. Accordingly, there are few long-term studies in northern high latitudes that capture interannual variability over a decade for comparison. Generally, these also show that interannual variability may not be as significant as variability among land cover types. In a 6-year eddy covariance study in upland tundra in interior Alaska, interannual variability in NEE was

~50% (Celis et al., 2017), larger than the interannual variability in this study but still smaller than variability among land cover types. However, further north in Alaskan tundra, interannual variability in growing season NEE over 8 years measured with eddy covariance was 13% (Euskirchen et al., 2017), slightly smaller than in this study or in the other interior Alaska site. In the North Slope tundra, interannual variability was correlated with the day of soil thaw (Euskirchen et al., 2017). Similarly, much of the interannual variability in modeled NEE in this study was due to differences in the timing of the onset of CO_2 uptake, as well as other growing season processes (Figure 7b).

Other studies have shown that nongrowing season emissions can be key to determining whether upland tundra is a net CO_2 sink or source (Natali et al., 2011). Capturing nongrowing season CO_2 emissions in another site on the North Slope of Alaska resulted in significant variability among land cover types measured annually (105%), while a comparison of growing season NEE showed only small variability among land cover types (14%; Euskirchen et al., 2017). In this study, the cold season fluxes resulted in differences in modeled NEE among land cover types (Figure 7a) but contributed little to the interannual variability of modeled NEE (Figure 7b). Modeled nongrowing season CH_4 flux measurements were also important for variability among land cover types in this study (Figure 7c), but not as important for interannual variability (Figure 7d), similar to recent findings across many sites (Treat, Bloom, & Marushchak, 2018).

In this study, the modeled decadal emissions overlapped with the few annual measurements of C exchange at this site. Our results showed a modeled regional net CO_2 uptake of -75 ± 12 g C m^{-2} year^{-1} (annual CO_2 flux: -39 to -100 g C m^{-2} year^{-1}), in general agreement with previous site measurements of -41 to -71 g C m^{-2} year^{-1} from 2007–08 (Marushchak et al., 2013). The modeled regionally weighted CH_4 fluxes in this study ranged from 2.1 to 4.8 g C m^{-2} year^{-1}, in general agreement with the previously reported 5.0 g C m^{-2} year^{-1} at this site (Marushchak et al., 2016).

Capturing the differences in land cover variability, particularly between uplands and wetlands, was key for accurate regional estimates of NEE within Seida. Despite a larger area of uplands (60%, including both forest and tundra) compared to wetlands in the Seida study region, uplands were responsible for only 33% of the areally weighted net C uptake (Table 2; Figure 8). The majority of the C uptake as NEE occurred in the permafrost peat plateaus (25%) and the permafrost-free fens (43%). In Northern Fennoscandia, peat plateaus are significant sinks of atmospheric CO_2, sequestering 46 g C m^{-2} year^{-1} (Olefeldt et al., 2012). In low-polygon tundra in Barrow, more productive vegetation was found in wetter tundra areas that developed in drained thaw lakes, resulting in a disproportionately large sink in a regional estimate of CO_2 exchange (Zulueta et al., 2011). However, CO_2 efflux from lakes at Barrow (16% of area) nearly offset the strong C uptake in the wet tundra vegetation types (VTLB, 51% of area), demonstrating that wetland and aquatic components of the landscape necessitate consideration in regional NEE (Sturtevant & Oechel, 2013).

The relative fraction of uplands and lowlands is also key for the regional CH_4 balance, both within Seida and across other tundra

sites. The total modeled CH_4 emissions from the fens at Seida in this study (17–22 g C m^{-2} year^{-1}) were large enough that fluxes were not offset by the small modeled net CH_4 uptake in the relatively well-drained soils that covered nearly 85% of the region (Figure 8b, Table 2). However, in lower resolution classification, the fraction of wetlands decreased as their patch size was frequently smaller than pixel size (Figures 2 and 8d). The reduced areal coverage of wetlands resulted in a significant (20%–60%) decrease in the regionally weighted CH_4 flux at Seida (Figure 8b,d), demonstrating the importance of accurately representing the spatial extent of wetlands when calculating regional CH_4 fluxes. Similar results were shown in a previous study where wetland area increased due to permafrost thaw, rather than decreased like in this study; a small increase in wetland area (~7%) resulted in a ~ 40% increase in the regional CH_4 flux (Christensen et al., 2004).

In a broader context, the regional landscape composition of uplands versus lakes and wetlands also has significant effects on regional CH_4 emissions. Across tundra sites, higher regional CH_4 emissions were found from regions with more lakes and wetlands than Seida, while lower regional CH_4 fluxes were found in regions with a smaller areal extent of wetlands and lakes, as well as in colder regions. A region with a greater abundance of lakes and wetlands (30% area vs. 15.5% in this study), the Yukon–Kuskokwim Delta in Alaska, had 75% higher regional fluxes than the modeled CH_4 fluxes in this study (Bartlett et al., 1992). On the other hand, the areally weighted CH_4 fluxes in tundra of the Kuparuk River Basin, North Slope, Alaska, were 80% lower, due to a 5× lower mean wetland CH_4 flux and smaller wetland extent (6% of the area) (Reeburgh et al., 1998). Colder temperatures may have resulted in the 32% smaller areally weighted CH_4 flux from Barrow tundra despite significant wetland and lake area (~67%) (Sturtevant & Oechel, 2013). Both the comparison among sites with regional CO_2 and CH_4 fluxes and the spatial analysis using lower resolution imaging (Figure 8) show similar results. This shows that differences in the relative fraction of wetland area versus upland area result in significant differences in regional C fluxes, including both CO_2 and CH_4, at this site and among Arctic tundra ecosystems.

4.2 | Using landscape heterogeneity to improve regional carbon flux estimates

In this study, regional estimates of C exchange were based on scaling measurements of individual land cover types based on vegetation composition using classifications at high spatial resolutions. A previous study in this region showed that a lower spatial resolution had little effect on total C pools, but had large effects on individual classes, most notably fen peatlands (Hugelius, 2012). Unlike total C pools, we showed here that the full C balance is highly sensitive to the representation of fen peatlands among spatial resolution in scaling (Figure 8). Lowering the spatial resolution of the regional C balance scaling introduced coefficients of variation exceeding 100% and 200% for CO_2 and CH_4, respectively. While the individual land cover types at this site reflect vegetation differences related to

topography, including drainage, mean water table position, and pH, this scaling approach may underestimate the effects of smaller variations due to microsite conditions or short-term climatic variability. For example, small-scale phenological differences as well as broader spatial differences can affect regional estimates of NEE (Vourlitis et al., 2003). In this study, similar C fluxes were modeled and measured at the independent calibration and validation sites, which indicates much of the small-scale variability was captured in our approach (Table A3, Figures A6–A8 in Supporting information Appendix S1). Ideally, future modeling efforts could incorporate more microsite variability, including factors such as lateral energy, water, and carbon transfer across the landscape.

Our findings support previous recommendations of land cover classifications using 30 m or finer resolutions (Bartsch et al., 2016; Davidson et al., 2017; Virtanen & Ek, 2014). Modeled net ecosystem exchange and CH_4 flux changed only slightly (≤5%) at 20 m pixel size compared to the 2.4 m resolution used as a default. This 20 m pixel size is approximately similar to spatial resolution of Landsat (30 m) and Sentinel-2 satellite imagery (10 m, four spectral bands; 20 m, extra six spectral bands). However, CH_4 emissions decreased substantially by 20%–40% even at an intermediate lower resolution such as 160 m (Figure 8), which is still finer than the resolution provided by Modis and AVHRR satellite imagery (pixel size ≥250 m). CO_2 emissions were not affected as strongly (Figure 8). Using lower resolution imagery may severely underestimate Arctic CH_4 emissions as many wetland areas may not be identified.

Our results have significant implications for the treatment of landscape scale heterogeneity in process-based models that run at regional to global spatial domains: using simple land cover classifications based on single (one) category and/or coarse resolution imagery could lead to significant biases in regional C emissions (Figure 8). Remedies include the implementation of different land cover types, especially wetlands and lakes, to represent the hot spots of C cycling in the landscape, which can be done using subgrid cell tiling methods. Alternatively, scaling based on maps of continuous variables, like leaf area index (Oechel et al., 2000; Vourlitis et al., 2003), or subpixel classification methods could be used, in which one pixel would include some proportions of several land cover types (Muster et al., 2013).

Our results clearly showed that net ecosystem CO_2 exchange and CH_4 fluxes differed significantly between wetlands and uplands and both were important components of the regional C balance. As such, we found that the relative fraction of uplands and wetlands within a region was key to determining the net ecosystem C exchange of both within this site, Seida, and across other regions of Arctic tundra. The variability in modeled C exchange among land cover types was much greater than the interannual variability (Figure 7). This study highlights that capturing the variability due to the full variety of land cover types is perhaps more important than conducting extended measurement campaigns over longer periods. Accurately characterizing the landscape composition, particularly between uplands and wetlands and lakes, is key to determining the net ecosystem C exchange in the changing Arctic.

ORCID

Claire C. Treat iD http://orcid.org/0000-0002-1225-8178
Carolina Voigt iD http://orcid.org/0000-0001-8589-1428
Zeli Tan iD http://orcid.org/0000-0001-5958-2584
Christina Biasi iD https://orcid.org/0000-0002-7413-3354

REFERENCES

Bartlett, K. B., Crill, P. M., Sass, R. L., Harriss, R. C., & Dise, N. B. (1992). Methane emissions from tundra environments in the Yukon-Kuskokwim Delta, Alaska. *Journal of Geophysical Research-Atmospheres*, 97, 16645–16660. https://doi.org/10.1029/91JD00610

Bartsch, A., Höfler, A., Kroisleitner, C., & Trofaier, A. (2016). Land cover mapping in northern high latitude permafrost regions with satellite data: Achievements and remaining challenges. *Remote Sensing*, 8, 979. https://doi.org/10.3390/rs8120979

Bruhwiler, L., Dlugokencky, E., Masarie, K., Ishizawa, M., Andrews, A., Miller, J., … Worthy, D. (2014). CarbonTracker-CH4: An assimilation system for estimating emissions of atmospheric methane. *Atmospheric Chemistry and Physics*, 14, 8269–8823.

Bubier, J. L., Moore, T. R., & Crosby, G. (2006). Fine-scale vegetation distribution in a cool temperate peatland. *Canadian Journal of Botany-Revue Canadienne De Botanique*, 84, 910–923. https://doi.org/10.1139/b06-044

Celis, G., Mauritz, M., Bracho, R., Salmon, V. G., Webb, E. E., Hutchings, J., … Schuur, E. A. (2017). Tundra is a consistent source of CO_2 at a site with progressive permafrost thaw during 6 years of chamber and eddy covariance measurements. *Journal of Geophysical Research: Biogeosciences*, 122, 1471–1485.

Christensen, T. R., Johansson, T., Åkerman, H. J., Mastepanov, M., Malmer, N., Friborg, T., … Svensson, B. H. (2004). Thawing sub-arctic permafrost: Effects on vegetation and methane emissions. *Geophysical Research Letters*, 31, L04501. https://doi.org/10.1029/2003GL018680

Christensen, T. R., Johansson, T., Olsrud, M., Ström, L., Lindroth, A., Mastepanov, M., … Callaghan, T. V. (2007). A catchment-scale carbon and greenhouse gas budget of a subarctic landscape. *Philosophical Transactions of the Royal Society a-Mathematical Physical and Engineering Sciences*, 365, 1643–1656. https://doi.org/10.1098/rsta.2007.2035

Cole, J. J., Prairie, Y. T., Caraco, N. F., McDowell, W. H., Tranvik, L. J., Striegl, R. G., … Melack, J. (2007). Plumbing the global carbon cycle: Integrating inland waters into the terrestrial carbon budget. *Ecosystems*, 10, 172–185. https://doi.org/10.1007/s10021-006-9013-8

Davidson, S., Santos, M., Sloan, V., Reuss-Schmidt, K., Phoenix, G., Oechel, W., & Zona, D. (2017). Upscaling CH_4 fluxes using high-resolution imagery in Arctic tundra ecosystems. *Remote Sensing*, 9, 1227. https://doi.org/10.3390/rs9121227

Euskirchen, E. S., Bret-Harte, M. S., Shaver, G. R., Edgar, C. W., & Romanovsky, V. E. (2017). Long-term release of carbon dioxide from Arctic tundra ecosystems in Alaska. *Ecosystems*, 20, 960–974. https://doi.org/10.1007/s10021-016-0085-9

Griffis, T. J., Rouse, W. R., & Waddington, J. M. (2000). Interannual variability of net ecosystem CO_2 exchange at a subarctic fen. *Global Biogeochemical Cycles*, 14, 1109–1121.

Hartmann, D. L., Tank, A. M. K., Rusticucci, M., Alexander, L. V., Brönnimann, S., Charabi, Y. A. R., … Soden, B. J. (2013). Observations: Atmosphere and surface. In T. F. Stocker, D. Qin, G.-K. Plattner, M. Tignor, S. K. Allen, J. Boschung, A. Nauels, Y. Xia, V. Bex, & P. M. Midgley (Eds.), *Climate change 2013 the Physical Science Basis: Working Group I Contribution to the Fifth Assessment Report of the Intergovernmental Panel on Climate Change*. Cambridge, UK: Cambridge University Press.

Heikkinen, J. E. P., Virtanen, T., Huttunen, J. T., Elsakov, V., & Martikainen, P. J. (2004). Carbon balance in East European tundra. *Global Biogeochemical Cycles*, 18, GB1023. https://doi.org/10.1029/2003GB002054

Hugelius, G. (2012). Spatial upscaling using thematic maps: An analysis of uncertainties in permafrost soil carbon estimates. *Global Biogeochemical Cycles*, 26, GB2026. https://doi.org/10.1029/2011GB004154

Hugelius, G., Routh, J., Kuhry, P., & Crill, P. (2012). Mapping the degree of decomposition and thaw remobilization potential of soil organic matter in discontinuous permafrost terrain. *Journal of Geophysical Research: Biogeosciences*, 117, G02030. https://doi.org/10.1029/2011JG001873

Hugelius, G., Virtanen, T., Kaverin, D., Pastukhov, A., Rivkin, F., Marchenko, S., … Kuhry, P. (2011). High-resolution mapping of ecosystem carbon storage and potential effects of permafrost thaw in periglacial terrain. European Russian Arctic. *Journal of Geophysical Research*, 116, G03024. https://doi.org/10.1029/2010JG001606

Jorgensen, C. J., Johansen, K. M. L., Westergaard-Nielsen, A., & Elberling, B. (2015). Net regional methane sink in High Arctic soils of northeast Greenland. *Nature Geoscience*, 8, 20–23. https://doi.org/10.1038/ngeo2305

Kling, G. W., Kipphut, G. W., & Miller, M. C. (1991). Arctic lakes and streams as gas conduits to the atmosphere: Implications for tundra carbon budgets. *Science*, 251, 298–301. https://doi.org/10.1126/science.251.4991.298

Koven, C. D., Ringeval, B., Friedlingstein, P., Ciais, P., Cadule, P., Khvorostyanov, D., … Tarnocai, C. (2011). Permafrost carbon-climate feedbacks accelerate global warming. *Proceedings of the National Academy of Sciences*, 108, 14769–14774. https://doi.org/10.1073/pnas.1103910108

Kurylyk, B. L., Hayashi, M., Quinton, W. L., Mckenzie, J. M., & Voss, C. I. (2016). Influence of vertical and lateral heat transfer on permafrost thaw, peatland landscape transition, and groundwater flow. *Water Resources Research*, 52, 1286–1305. https://doi.org/10.1002/2015WR018057

Lafleur, P. M., Griffis, T. J., & Rouse, W. R. (2001). Interannual variability in net ecosystem CO2 exchange at the arctic treeline. *Arctic Antarctic and Alpine Research*, 33, 149–157.

Lafleur, P. M., & Humphreys, E. R. (2007). Spring warming and carbon dioxide exchange over low Arctic tundra in central Canada. *Global Change Biology*, 14, 740–756. https://doi.org/10.1111/j.1365-2486.2007.01529.x

Li, C., Aber, J., Stange, F., Butterbach-Bahl, K., & Papen, H. (2000). A process-oriented model of N_2O and NO emissions from forest soils: 1. Model development. *Journal of Geophysical Research: Atmospheres*, 105, 4369–4384.

Marushchak, M. E., Friborg, T., Biasi, C., Herbst, M., Johansson, T., Kiepe, I., … Søgaard, H. (2016). Methane dynamics in the subarctic tundra: Combining stable isotope analyses, plot- and ecosystem-scale flux measurements. *Biogeosciences*, 13, 597–608. https://doi.org/10.5194/bg-13-597-2016

Marushchak, M. E., Kiepe, I., Biasi, C., Elsakov, V., Friborg, T., Johansson, T., … Martikainen, P. J. (2013). Carbon dioxide balance of subarctic tundra from plot to regional scales. *Biogeosciences*, 10, 437–452. https://doi.org/10.5194/bg-10-437-2013

Marushchak, M. E., Pitkamaki, A., Koponen, H., Biasi, C., Seppälä, M., & Martikainen, P. J. (2011). Hot spots for nitrous oxide emissions found in different types of permafrost peatlands. *Global Change Biology*, 17, 2601–2614. https://doi.org/10.1111/j.1365-2486.2011.02442.x

Mastepanov, M., Sigsgaard, C., Dlugokencky, E. J., Houweling, S., Strom, L., Tamstorf, M. P., & Christensen, T. R. (2008). Large tundra methane burst during onset of freezing. *Nature*, 456, 628–U658. https://doi.org/10.1038/nature07464

Mastepanov, M., Sigsgaard, C., Tagesson, T., Ström, L., Tamstorf, M. P., Lund, M., & Christensen, T. R. (2013). Revisiting factors controlling methane emissions from high-Arctic tundra. *Biogeosciences*, 10, 5139–5158. https://doi.org/10.5194/bg-10-5139-2013

McGuire, A. D., Christensen, T. R., Hayes, D. J., Heroult, A., Euskirchen, E., Yi, Y., … Oechel, W. (2012). An assessment of the carbon balance of Arctic tundra: Comparisons among observations, process models, and atmospheric inversions. *Biogeosciences*, 9, 3185–3204. https://doi.org/10.5194/bg-9-3185-2012

Miller, P. A., & Smith, B. (2012). Modelling tundra vegetation response to recent arctic warming. *Ambio*, 41, 281–291. https://doi.org/10.1007/s13280-012-0306-1

Muster, S., Heim, B., Abnizova, A., & Boike, J. (2013). Water body distributions across scales: A remote sensing based comparison of three arctic tundra wetlands. *Remote Sensing*, 5(4):1498–1523.

Myhre, G., Shindell, D., & Bréon, F.-M. et al. (2013). Anthropogenic and natural radiative forcing. In T. F. Stocker, D. Qin, G.-K. Plattner, M. Tignor, S. K. Allen, J. Boschung, A. Nauels, Y. Xia, V. Bex, & P. M. Midgley (Eds.), *Climate change 2013: The physical science basis. Contributions of Working Group I to the Fifth Assessment Report of the Intergovernmental Panel on Climate Change*. Cambridge, UK and New York, NY: Cambridge University Press.

Natali, S. M., Schuur, E. A. G., Trucco, C., Pries, C. E. H., Crummer, K. G., & Lopez, A. F. B. (2011). Effects of experimental warming of air, soil and permafrost on carbon balance in Alaskan tundra. *Global Change Biology*, 17, 1394–1407. https://doi.org/10.1111/j.1365-2486.2010.02303.x

Oberbauer, S. F., Tweedie, C. E., Welker, J. M., Fahnestock, J. T., Henry, G. H., Webber, P. J., … Starr, G. (2007). Tundra CO_2 fluxes in response to experimental warming across latitudinal and moisture gradients. *Ecological Monographs*, 77, 221–238.

Oechel, W. C., Vourlitis, G. L., Verfaillie, J., Crawford, T., Brooks, S., Dumas, E., … Zulueta, R. (2000). A scaling approach for quantifying the net CO_2 flux of the Kuparuk River Basin, Alaska. *Global Change Biology*, 6, 160–173.

Olefeldt, D., Roulet, N. T., Bergeron, O., Crill, P., Bäckstrand, K., & Christensen, T. R. (2012). Net carbon accumulation of a high-latitude permafrost palsa mire similar to permafrost-free peatlands. *Geophysical Research Letters*, 39, L03501. https://doi.org/10.1029/2011GL050355

Olefeldt, D., Turetsky, M. R., Crill, P. M., & McGuire, A. D. (2013). Environmental and physical controls on northern terrestrial methane emissions across permafrost zones. *Global Change Biology*, 19, 589–603.

Reeburgh, W. S., King, J. Y., Regli, S. K., Kling, G. W., Auerbach, N. A., & Walker, D. A. (1998). A CH_4 emission estimate for the Kuparuk River basin, Alaska. *Journal of Geophysical Research-Atmospheres*, 103, 29005–29013.

Repo, M. E., Huttunen, J., Naumov, A., Chichulin, A., Lapshina, E., Bleuten, W., & Martikainen, P. (2007). Release of CO_2 and CH_4 from small wetland lakes in western Siberia. *Tellus Series B*, 59, 788–796.

Schneider, J., Grosse, G., & Wagner, D. (2009). Land cover classification of tundra environments in the Arctic Lena Delta based on Landsat 7 ETM+ data and its application for upscaling of methane emissions. *Remote Sensing of Environment*, 113, 380–391. https://doi.org/10.1016/j.rse.2008.10.013

Smith, B., Prentice, I. C., & Sykes, M. T. (2001). Representation of vegetation dynamics in the modelling of terrestrial ecosystems: Comparing two contrasting approaches within European climate space. *Global Ecology and Biogeography*, 10, 621–637. https://doi.org/10.1046/j.1466-822X.2001.00256.x

Sturtevant, C. S., & Oechel, W. C. (2013). Spatial variation in landscape-level CO_2 and CH_4 fluxes from arctic coastal tundra: Influence from vegetation, wetness, and the thaw lake cycle. *Global Change Biology*, 19, 2853–2866.

Tan, Z., Zhuang, Q., Shurpali, N. J., Marushchak, M. E., Biasi, C., Eugster, W., & Walter Anthony, K. (2017). Modeling CO_2 emissions from Arctic lakes: Model development and site-level study. *Journal of Advances in Modeling Earth Systems*, 9(5), 2190–2213.

Tan, Z., Zhuang, Q., & Walter Anthony, K. (2015). Modeling methane emissions from arctic lakes: Model development and site-level study. *Journal of Advances in Modeling Earth Systems*, 7, 459–483. https://doi.org/10.1002/2014MS000344

Treat, C. C., Bloom, A. A., & Marushchak, M. E. (2018). Nongrowing season methane emissions–a significant component of annual emissions across northern ecosystems. *Global Change Biology*, 24, 3331–3343.

R Development Core Team (2008). *R: A language and environment for statistical computing*. Vienna, Austria: R Foundation for Statistical Computing.

Virtanen, T., & Ek, M. (2014). The fragmented nature of tundra landscape. *International Journal of Applied Earth Observation and Geoinformation*, 27, 4–12. https://doi.org/10.1016/j.jag.2013.05.010

Voigt, C., Lamprecht, R. E., Marushchak, M. E., Lind, S. E., Novakovskiy, A., Aurela, M., … Biasi, C. (2017). Warming of subarctic tundra increases emissions of all three important greenhouse gases – carbon dioxide, methane, and nitrous oxide. *Global Change Biology*, 23, 3121–3138. https://doi.org/10.1111/gcb.13563

Vourlitis, G. L., Verfaillie, J., Oechel, W. C., Hope, A., Stow, D., & Engstrom, R. (2003). Spatial variation in regional CO_2 exchange for the Kuparuk River Basin, Alaska over the summer growing season. *Global Change Biology*, 9, 930–941. https://doi.org/10.1046/j.1365-2486.2003.00639.x

Walker, D. A., Raynolds, M. K., Daniëls, F. J., Einarsson, E., Elvebakk, A., Gould, W. A., … Moskalenko, N. G. (2005). The Circumpolar Arctic vegetation map. *Journal of Vegetation Science*, 16, 267–282. https://doi.org/10.1111/j.1654-1103.2005.tb02365.x

Wania, R., Ross, I., & Prentice, I. C. (2009). Integrating peatlands and permafrost into a dynamic global vegetation model: 2. Evaluation and sensitivity of vegetation and carbon cycle processes. *Global Biogeochemical Cycles*, 23, GB3014.

Wania, R., Ross, I., & Prentice, I. C. (2010). Implementation and evaluation of a new methane model within a dynamic global vegetation model: LPJ-WHyMe v1.3.1. *Geoscientific Model Development*, 3, 565–584. https://doi.org/10.5194/gmd-3-565-2010

Wolf, A., Callaghan, T. V., & Larson, K. (2008). Future changes in vegetation and ecosystem function of the Barents Region. *Climatic Change*, 87, 51–73. https://doi.org/10.1007/s10584-007-9342-4

Zhang, Y., Chen, W. J., & Cihlar, J. (2003). A process-based model for quantifying the impact of climate change on permafrost thermal regimes. *Journal of Geophysical Research-Atmospheres*, 108, 4695. https://doi.org/10.1029/2002JD003354

Zhang, W., Miller, P. A., Smith, B., Wania, R., Koenigk, T., & Döscher, R. (2013). Tundra shrubification and tree-line advance amplify arctic

climate warming: Results from an individual-based dynamic vegetation model. *Environmental Research Letters*, 8, 034023. https://doi.org/10.1088/1748-9326/8/3/034023

Zhang, Y., Sachs, T., Li, C., & Boike, J. (2012). Upscaling methane fluxes from closed chambers to eddy covariance based on a permafrost biogeochemistry integrated model. *Global Change Biology*, 18, 1428–1440. https://doi.org/10.1111/j.1365-2486.2011.02587.x

Zhuang, Q., Zhu, X., He, Y., Prigent, C., Melillo, J. M., McGuire, A. D., … Kicklighter, D. W. (2015). Influence of changes in wetland inundation extent on net fluxes of carbon dioxide and methane in northern high latitudes from 1993 to 2004. *Environmental Research Letters*, 10, 095009. https://doi.org/10.1088/1748-9326/10/9/095009

Zulueta, R. C., Oechel, W. C., Loescher, H. W., Lawrence, W. T., & Paw, U. K. T. (2011). Aircraft-derived regional scale CO_2 fluxes from vegetated drained thaw-lake basins and interstitial tundra on the Arctic Coastal Plain of Alaska. *Global Change Biology*, 17, 2781–2802. https://doi.org/10.1111/j.1365-2486.2011.02433.x

SUPPORTING INFORMATION

Additional supporting information may be found online in the Supporting Information section at the end of the article.